MATERIALE PLASTICE
https://revmaterialeplastice.ro
https://doi.org/10.37358/Mat.Plast.1964

Influence of Hot-Air Jet (HAJ) Additional Heat Source on the Deposited Polymer in FFF Printing

REMUS SOCOL[1], IULIANA DUMA[2], IULIAN STEFAN[1], IONEL-DANUT SAVU[1,2*], NICUSOR-ALIN SIRBU[2], SORIN VASILE SAVU[1,2], MARIN-ANDRETTI CIUNGU[1]
[1]University of Craiova, Faculty of Mechanics, Department of EMTS, 1 Calugareni Str., 220037, Drobeta-Turnu Severin, Romania
[2]NRDI for Welding and Material Testing, 30 Mihai Viteazu Blvd., 300222, Timisoara, Romania

Abstract: *The paper presents part of the results of larger research aimed at evaluating the possibility of improving the characteristics of the FFF printed product by using hybrid heating sources. The results presented aim at the influence of the cooling rate on the characteristics of parts manufactured by 3D FFF printing from Polylactic acid (PLA), with a focus on the structural, thermal and mechanical properties, when the additional heat source is represented by a hot air jet. Microscopic analysis showed that rapid cooling generates a more irregular texture, poor interlayer adhesion and a rougher surface, while slow cooling ensures a uniform texture, improved interlayer adhesion and fewer defects. From a thermal point of view, the glass transition temperature (T_g) was slightly higher for the slowly cooled samples, due to the relaxation of internal stresses. The crystallization temperature (T_c) increased progressively with the reduction of the cooling rate, indicating a higher initial crystallinity, and the energy associated with the crystallization reaction decreased. The melting temperature (T_m) showed minimal variations, but the melting enthalpy was higher for the slowly cooled samples, reflecting better organized crystals. Mechanical properties revealed that the rapidly cooled parts have higher stiffness at low temperatures, due to internal stresses, but brittle behaviour. The slowly cooled parts showed higher stiffness at high temperatures and ductile behaviour, with progressive deformations before fracture, due to the relaxation of internal stresses and the formation of partial crystals. The results emphasize the importance of controlling the cooling rate in the FFF process to optimize the interlayer adhesion, mechanical properties and thermal stability of the printed parts, allowing to adapt their performance to specific application requirements.*

Keywords*: additional heating source, 3D printing, glass transition, storage modulus, DSC analysis*

1. Introduction

3D printing is a family of manufacturing processes that differ from traditional processes by which material is sampled to obtain the desired shapes and sizes. 3D printing adds material, in a controlled manner, to generate complex shapes, which are difficult to generate by other methods, especially subtractive ones [1]. With a history of approximately 70-80 years, 3D printing has experienced important development in the last 15 years, mainly due to the fact that many of the patented inventions from the 80s, which were the basis for the development of the processes, have become public [2]. Being public, innovators around the world have developed, starting from them, various solutions for depositing polymeric, metallic, ceramic or composite materials.

The 3D printing process Fused Filament Fabrication (FFF) is one of the most widely used additive manufacturing processes, its products covering a very large number of areas, and the filler materials can be, practically, any type of thermoplastic polymer, or at least most of them [2].

Like any technological process, it is defined by a series of parameters whose values influence the result of the process application [1-6]. These parameters are chosen depending on the material used to deposit and the desired productivity and quality to be obtained (i.e. for high productivity a lower resolution and higher speed can be used, while for a high quality a higher resolution is required).

**email: ionel.savu@edu.ucv.ro*

Among the polymers that have given very good results as additive materials, the most used are Polylactic acid (PLA), Acrylonitrile butadiene styrene (ABS), Polyether ether ketone (PEEK), Polyethylene terephthalate glycol (PET-G) and Polypropylene carbonate (PPC) [1, 3, 4, 7]. Each of these polymers has its own thermal characteristics (temperature of glass transition - T_g, temperature of cold crystallization - T_c, melting temperature - T_m, specific heat flow rate) [1, 3, 8-13]. Each has specific mechanical characteristics (storage modulus, loss modulus, and $Tan\ \delta$) [1, 3, 10, 13-18]. The parameters of the 3D printing process influence all of these characteristics of the polymer, so products made by printing can have various characteristics, depending on the conditions in which the process takes place.

The typical configuration of equipment used in the FFF printing process does not allow precise control over the cooling rate of the deposited polymer [1, 3]. Knowing the physical and mechanical characteristics of polymers, as well as the factors that influence these characteristics, it is predicted that controlling the cooling rate of the deposited polymer can influence several characteristics of the material [5].

A slower cooling of the deposited material should allow it to remain in the viscous fluid state for longer, promoting a better diffusion of the polymer chains across the layer interfaces [5, 17, 18]. This results in an interlayer weld with higher strength, reducing the probability of delamination and increasing the overall mechanical strength [5, 17-19]. A rapid cooling will cause uneven shrinkage, which leads to residual stresses and potential deformations of the printed product [5, 17, 18]. A slower cooling should reduce these thermo-physical stresses specific to cooling shrinkage, improving dimensional stability and part accuracy [5, 17, 18].

Starting from the real premise that there are stresses in the deposited material due to at least the extrusion process, a rapid cooling can have an effect in blocking internal stresses. These cannot be distributed in the material, making the product brittle. By reducing the cooling rate there is a real possibility to balance the hardness values with those of the ductility characteristics. For semi-crystalline polymers, often used in FFF printing, such as PLA or PEEK, a slower cooling should provide more time for the polymer chains to arrange themselves into crystalline structures [8, 9, 12]. Higher crystallinity usually improves mechanical properties such as stiffness and strength, although it can reduce ductility. If a slow cooling rate is provided, the molten polymer has more time to flow and level out, which should result in a smoother surface finish [5, 10, 20]. This is particularly beneficial for applications where aesthetic quality is critical. A gradual cooling reduces thermal gradients that contribute to shrinkage and, consequently, material deformation. This is particularly important for larger printed products or products with high geometric complexity [5, 17-19].

We conclude that when talking about influences in a technical field, it is obvious that these influences cannot only be positive. One negative influence direction produced by the decrease in the cooling rate of the deposited polymer is related to an important economic aspect, namely the printing time. A disadvantage of a slow cooling rate is the longer printing time, as the part may require additional time to solidify before subsequent layers can be deposited effectively.

Two other negative aspects could be mentioned, but they are of a particular nature and are not considered when designing an FFF printing technology for the realization of common products. In the case of amorphous polymers such as PETG, slower cooling can affect the optical properties. Slow cooling speed can lead to a less transparent part due to increased relaxation of the polymer during cooling [21].

And in the case of polymers that are sensitive to thermal degradation, prolonged exposure to high temperatures can lead to degradation or discoloration if cooling is too slow. In this case, controlling the cooling cycle is essential to reduce the risk of thermal degradation during printing [22].

Thus, our research started with prediction that controlling the cooling rate in the sense of reducing it can significantly improve the quality, durability and mechanical performance of FFF printed parts, but requires careful optimization based on the material properties and application requirements.

Starting with these assumptions resulting not from an empirical evaluation, but more from a logic of the existing knowledge regarding the behaviour of polymers upon heating and cooling, it was desired to

experimentally verify some of the assumptions defined above.

Using an additional heat source in order to reduce the cooling rate of the deposited polymer, evaluations of the aesthetic and mechanical characteristics of the printed product were carried out. The additional heat source was a jet of hot air whose temperature was controlled in such a way as to maintain the deposited material in the viscous fluid state for longer.

2. Materials and methods

2.1. Equipment and materials

The experimental program consisted of 3D printing a parallelepiped-shaped part, the printing process being accompanied by additional heating using a hot air jet. The 3D printer was a commercial one from the Creality family (Ender 3), modified to attach an air jet supply circuit (Figure 1) heated with a resistive thermal source. The hot air jet source used - an Erbauer heat gun (Figure 2) - allowed for the adjustment of both the airflow rate (0-30 m³/h, measured with an LT LM-8000A anemometer, Figure 3) and the temperature (50-650°C) at the inlet of the supply circuit.

Figure 1. Creality Ender 3 printer modified by adding new heating source

Figure 2. Devices used to set the equipment for experiments

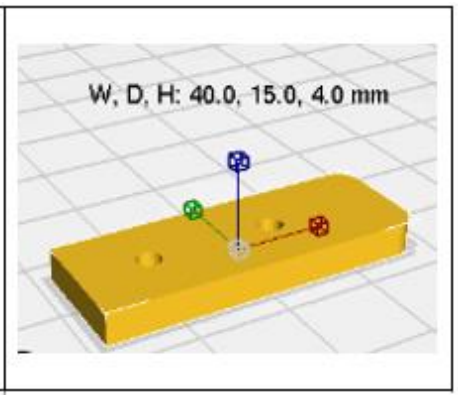

Figure 3. Design of the piece to print

The part was designed using the ANSYS Workbench FEA application (2012), the result being converted to *.stl format for communication with the printer.

The material used for deposition was a commercial filament (Polymaker PolyTerra PLA Charcoal Black) made of PLA, with a diameter of 1.75 mm.

2.2. Printing and heat addition parameters

The choice of printing process parameters was made based on the recommendation of the printing equipment manufacturer for 1.75 mm diameter PLA filament. They are presented in Table 1.

Table 1. Printing parameters used in the experimental program

Printing parameters				
Extrusion temperature (°C)	Bed deposition temperature (°C)	Infill density (%)	Printing speed (mm/s)	Shell thickness (mm)
220	70	50	100	0.9

The parameters of the additional source were established after analytical evaluations of the hot air jet flow and measurements of the air temperature at the exit of the guide circuit. The hot air jet was intended to have a laminar flow and to have at the exit point a controlled temperature of min 100°C. This temperature resulted from the balance of enthalpies during the cooling process, according to our theoretical considerations presented below.

$$H_{total} = H_{melting} + H_{HAJ} \quad (1)$$

where H_{HAJ} is the extra participation on enthalpy of the hot-air jet, during the heating of the polymer. That enthalpy can be quantified taking account that is directional:

$$H_{HAJ} = \frac{\frac{\partial Q_{HAJ}}{\partial x}}{V_{hp}} \quad (2)$$

and covers a specific volume of the printed product (V_{hp}).

In the same time, the cooling of the printed piece, in such convection heating, is governed by the Newton law, expressed for a cooling process:

$$Q = h \cdot A \cdot \Delta T \cdot \Delta t \quad (3)$$

where Q is the amount of heat transferred over time Δt, h is the heat transfer coefficient, A is the surface area of the part, and ΔT is the temperature difference between the part surface and the ambient air. To control the cooling rate, it is necessary a heat transfer rate of:

$$\dot{Q} = m \cdot c \cdot \dot{T} \quad (4)$$

where $\dot{Q}$ is the heat flux in W, m is the mass of the printed piece, c is the specific heat capacity, and $\dot{T}$ is the desired rate of temperature change. The additional heat must compensate for the reduction in the natural heat flux ($\dot{Q}_{naturally}$) of the part:

$$\dot{Q}_{addition} = \dot{Q}_{naturally} - m \cdot c \cdot \dot{T}_{reduced} \quad (5)$$

For a printed piece having a mass of 50 g, and a surface for convection of 1000 mm^2, using the heat capacity of PLA polymer of 1500 J/kg·K, and a convection coefficient of 25 W/m^2·K, to reduce the cooling rate with $\dot{T} = 40 \frac{grdC}{min} = 0.66 \frac{K}{s}$ is necessary a heat transfer of $\dot{Q} = 49.95\ W$, and a $\dot{Q}_{naturally} = 1.25\ W$. Subsequently, the additional heat results in: $\dot{Q}_{addition} = 48.7\ W$.

The temperature of the hot-air jet should be correlated to the laminar flowing, which is obtained for a Reynolds number below 2300.

In conclusion the minimum temperature of the hot-air jet to the entrance of the guiding circuit should be higher with 35ºC comparing to the exit temperature, so 135ºC.

2.3. Method

The experiment consisted of 3D printing the designed part type, the printing being accompanied by additional heating provided by the device attached to the Creality Ender 3 printer (Figure 4). Samples were made with additional heating of 100ºC, 120ºC and 140ºC, the purpose of the additional heating being to reduce the cooling rate of the material deposited by printing.

The parts made by 3D printing were measured according to ISO 1923:1999 regarding determination of linear dimensions to verify compliance with the initial design and to determine the influence of reducing the cooling rate on the residual deformations of the printed material.

The material deposited by printing was subjected to Differential Scanning Calorimetry (DSC) analysis according to ASTM E794-06 (2018) which is the standard dedicated to the test method for melting and crystallization temperatures by thermal analysis in order to evaluate the changes introduced by the additional heat source. DSC analysis was performed with NETZSCH HP Phoenix 204 (2011) equipment (Figure 5), in an inert atmosphere.

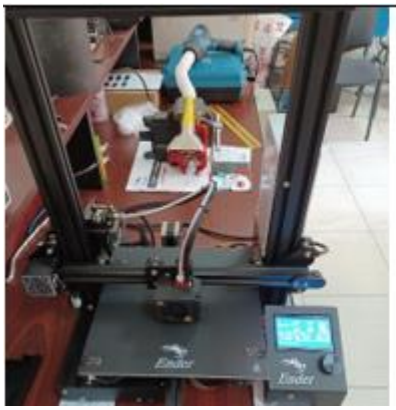

Figure 4. Creality Ender 3 printer modified for hybrid heating with additional hot-air jet

Figure 5. NETZSCH HP Phoenix 204 for DSC thermal analysis

Dynamic mechanical analysis (DMA) was also performed to determine the changes in the storage modulus (E′) and the damping coefficient ($Tan\ \delta$) according to the reference standard: ISO 6721-11:2019.

3. Results and discussions

Samples with masses ranging from 7…10 mg were taken from the 3D printed parts (Figure 6) and heated in a nitrogen environment to 300°C (initial temperature T_{min}=-50°C, T_o=50°C, T_{max}=300°C) at a heating rate of 10°C/min (ISO 11357-1:2023). They were held at this temperature for 2 min to erase the thermal history, after which they were cooled and reheated under the same conditions. The analysis was performed three times for each of the samples additionally heated with a hot air jet and the average results are reported in the paper (the variations of the results were below 1.7% for all measured quantities). In the second heating, the glass transition temperatures (T_g), cold crystallization temperatures (T_c), and melting temperatures (T_m) were determined. The enthalpies of melting and cold crystallization of the samples were also measured.

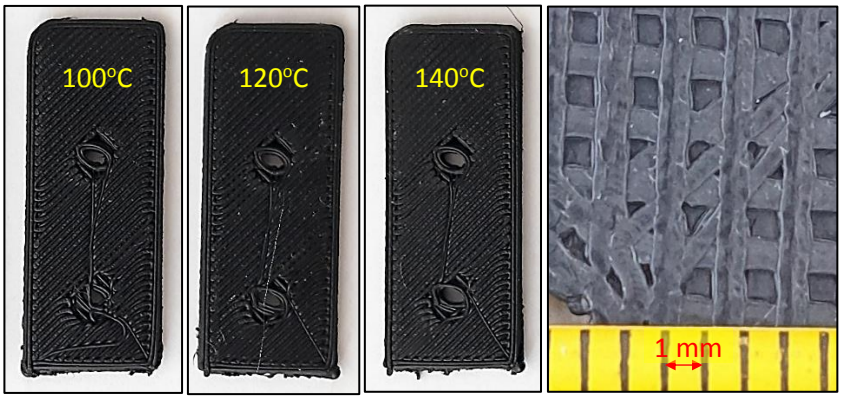

a. b. c. d.

Figure 6. Examples of samples printed using heat addition of 100°C (a), 120°C (b), and 140°C (c), as well as a magnification of the first deposited layer of the piece printed with 140°C heat addition

3.1. Dimensional compliance

The overall dimensions of the printed products were verified, measurements being made with devices with scales of the order of tens of micrometre. Three determinations were performed for each dimension. In the case of the hole diameter, it was measured the highest and the lowest diameters. The differences between the measured dimensions and those in the design are presented in Table 2.

Table 2. Differences between the design and the actual dimensions (according to EN ISO 1923:1999)[23]

Probe	Dimensions			
	ΔL (mm)	ΔW (mm)	ΔS (mm)	ΔD_1 / ΔD_2 (mm/mm)
No heat addition probe	0.78 0.76 0.75	0.63 0.69 0.62	0.44 0.44 0.45	0.12/-0.12 0.16/-0.12 0.15/-0.13
100ºC heat addition probe	0.75 0.73 0.75	0.61 0.62 0.62	0.40 0.41 0.39	0.10/-0.08 0.11/-0.09 0.11/-0.09
130ºC heat addition probe	0.71 0.72 0.73	0.58 0.57 0.61	0.41 0.41 0.39	0.10/-0.08 0.11/-0.08 0.09/-0.07
140ºC heat addition probe	0.71 0.71 0.74	0.60 0.60 0.58	0.38 0.41 0.38	0.10/-0.09 0.09/-0.07 0.09/-0.07
Note: 1. L-length, W-width, S-thickness, D_1 / D_2 - diameters of holes				

It is found that the dimensional differences between the four types of samples are small enough to be accepted as negligible. Therefore, the influence of the cooling rate on the residual deformations is insignificant, at least at the level of the overall dimensions of the 3D printed parts.

3.2 Macroscopic analysis

Visual analysis was performed with a TESCAN VEGA 3 microscope, a Scanning Electron Microscope (SEM) of the 4th generation. Magnifications of 14.2x and 35.5x were used for better evaluation.

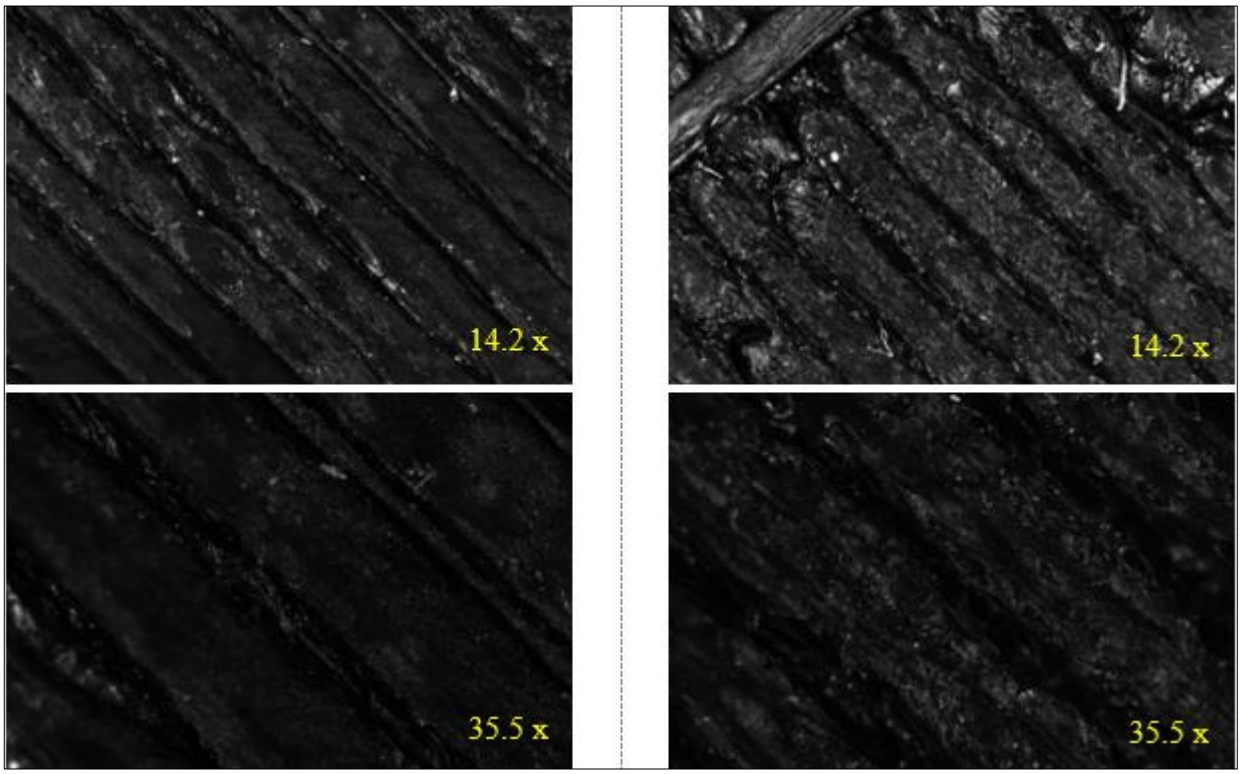

a. Sample without heat addition b. Sample with heat addition (120ºC)

Figure 7. SEM images of the samples

In the case of FFF deposition in the classical regime the texture appears more irregular, with a weaker

bond between the layers. More pronounced separation zones or lines between the layers are observed, indicating that the material did not have enough time to diffuse between the filaments. The surface is rougher and more uneven, which may be caused by rapid cooling that limits optimal layer fusion.

In the case of FFF deposition at a slower cooling rate, the texture is more uniform and the separation lines between the layers are less pronounced. The adhesion between the layers appears stronger, indicating that the material has had more time to fuse due to the slower cooling. The surface is smoother, with fewer defects or voids, reflecting a more uniform solidification process.

Therefore, the main differences found are related to interlayer bonding (in classical deposition, rapid cooling prevents efficient diffusion at the layer interface, leading to poor adhesion; in slow cooling deposition, the additional cooling time allows molecules to diffuse better, creating a stronger bond between the layers), surface roughness (rapid cooling leads to uneven shrinkage and more visible defects on the surface. Slow cooling minimizes rapid shrinkage and allows for a more uniform surface formation) and mechanical strength (classical deposition is more prone to interlayer fractures due to weak bonds; slow cooling deposition would be more mechanically resistant due to stronger interlayer bonds.) Overall, slower cooling improves the quality of the part by increasing the adhesion between the layers and reducing surface defects.

3.3. Influence on the melting and crystallization

The glass transition temperature (T_g) varies between approximately 63.2 °C and 64.7 °C for different conditions, according ISO 6721-11:2019 [24]. The slight increase in T_g for the curves of samples with additional heat (e.g.: +140 °C) can be explained by a greater relaxation of the polymer chains. The additional heating allows the release of accumulated internal stresses, which stabilizes the structure. The polymer with natural cooling (dotted line) has a lower T_g, indicating a more disordered structure (Figure 8), according ASTM E794-06 [25].

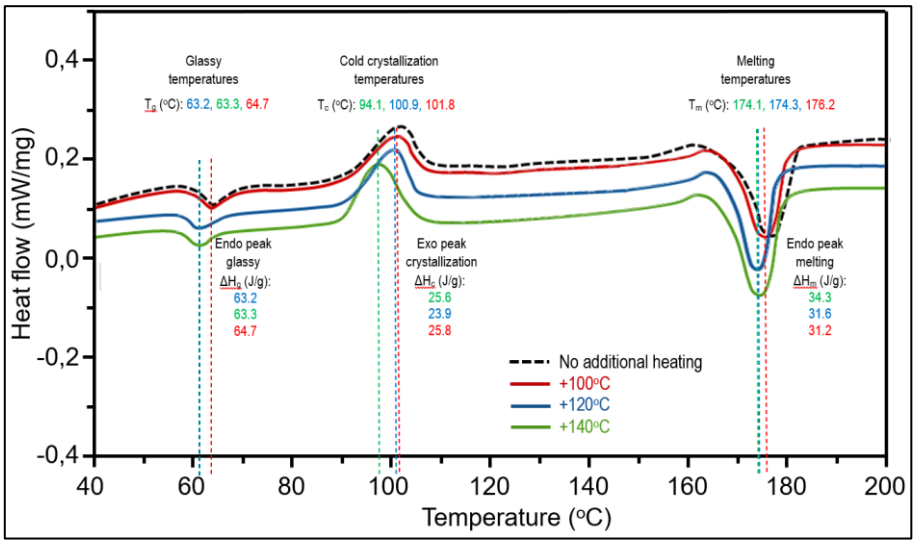

Figure 8. DSC curves for the four methods of polymers deposition, according ISO 11357-1:2023 [26]

Regarding cold crystallization, the critical crystallization temperature (T_c) has lower values for samples without additional heat and increases progressively for additional heating (+100°C, +120°C, +140°C). The values range between 94.1°C and 101.8°C.

The associated exothermic reaction energy (ΔT) decreases as the preheating temperature increases. Additional heating favours the initial crystallization of the polymer, reducing the amount of amorphous material that can crystallize in the cold. Therefore, the exotherm energy decreases. Samples without additional heating have more amorphous material, requiring more energy for crystallization.

The recorded values for the melting point (T_m) vary slightly between 174.1°C and 176.2°C, with minor changes between curves. The associated endothermic energy (ΔH_m) is slightly higher for the curves with additional heating (+120°C and +140°C), reflecting better organization of the crystals. Additional heating causes the formation of more stable and better-defined crystals, which require more energy to melt.

Therefore, the differences between the curves concern chain relaxation (preheating allows for the relaxation of internal stresses, slightly increasing T_g), crystallization (curves with additional heating have less cold crystallization, indicating a higher degree of initial crystallinity), and last but not least, the melting point (crystals formed at higher temperatures are better organized, leading to a pronounced endotherm).

3.4. Influence on the storage modulus and $Tan\ \delta$ ratio

Up to a temperature of approximately 43°C, the polymer deposited without heat addition has a higher storage modulus (Figure 9). This reveals a more ordered structure, but also residual internal stresses. These internal stresses contribute to an apparently higher stiffness at low temperatures.

At the same time, faster cooling leads to higher mechanical strength in the low temperature range. Above 43°C, the deposited polymer has a higher storage modulus, which shows a relaxation of the residual internal stresses, and the solidified polymer acquires a relaxed structure, with more stable intermolecular bonds. During slow cooling, the deposited polymer can undergo partial crystallization in a larger volume, which gives it a higher stiffness above 43°C, when the material starts to be more sensitive to the relaxation of the amorphous chains. In addition, being in the fluid-viscous state for a longer time, the deposited polymer has the opportunity to achieve better cohesion between the polymer chains at the contact points, which contributes to a higher modulus at high temperatures.

The temperature of 43°C can be associated with a specific transition, such as the beginning of the mobility of the amorphous segments in PLA. Up to this temperature, the stiffer structure and internal stresses in the deposited polymer without additional heating dominate the mechanical behaviour. Above this temperature, the deposited structure of the solidified polymer becomes more stable and stronger due to crystallization or better intermolecular interactions between the polymer layers.

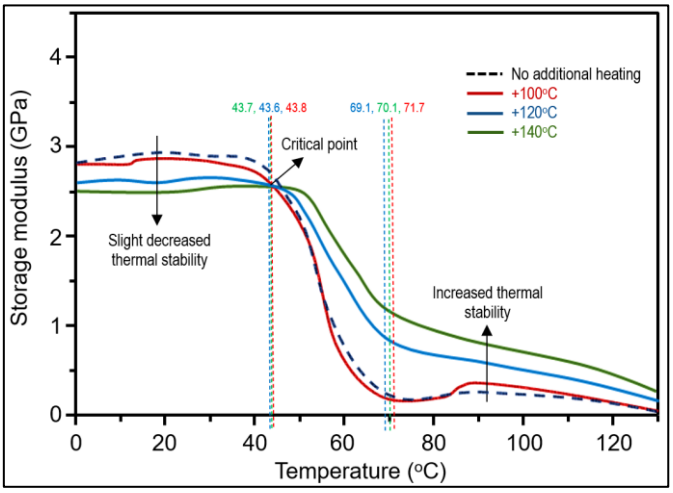

Figure 9. Storage modulus of the deposited polymers

This behaviour indicates that the polymer deposited without additional heating is more suitable for applications requiring stiffness at low temperatures, while the polymer deposited is more effective at higher temperatures.

Since the variation of $Tan\ \delta$ (the ratio of storage modulus to loss modulus) reflects the viscoelastic properties of PLA and provides insight into the balance between its elastic (storage modulus) and viscous (loss modulus) behaviour, it was considered necessary to analyse this indicator as well.

Figure 10 shows the $Tan\ \delta$ curves for the four states of the polymer.

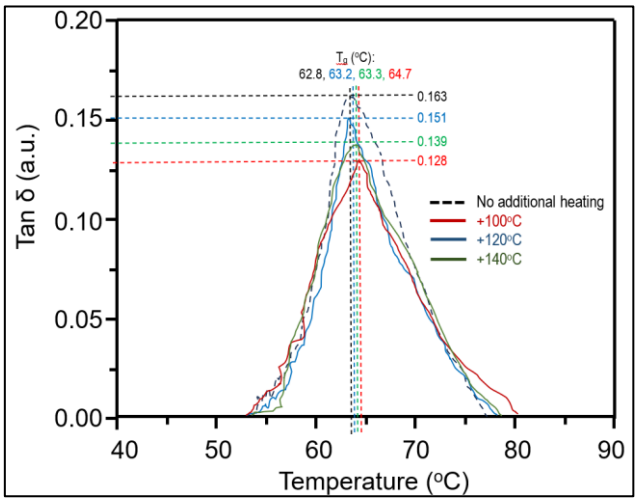

Figure 10. $Tan\ \delta$ graphs

The peak of the $Tan\ \delta$ curve usually corresponds to the glass transition temperature, which is visible on the graphs.

In the case of naturally cooled PLA the $Tan\ \delta$ peak is the highest and widest of all the curves. This indicates a higher damping capacity and a more amorphous structure. The rationale for this shape of the curve is that rapid cooling prevents the formation of crystalline regions, resulting in a predominantly amorphous PLA. The absence of ordered domains allows for more energy dissipation during deformation. The amorphous structure of the polymer maximizes molecular mobility and energy dissipation at the glassy temperature, T_g.

In the case of slow-cooled PLA curves, as the cooling rate decreases, the peak becomes sharper and shifts slightly higher in temperature. The height of the peak decreases with slower cooling rates. The reason is related to the fact that slower cooling allows the development of crystalline regions. The crystalline domains restrict molecular motion, reducing the damping capacity and narrowing the transition region. In other words, the crystalline regions act as physical cross-links, reducing molecular motion and energy dissipation. This results in a lower and sharper $Tan\ \delta$ peak at a slightly higher T_g temperature.

3.5. Behaviour during compression tests

The compression test was applied according to EN 2850 Method B / ASTM D695-23 dedicated to the The compression test was applied according to EN 2850 Method B / ASTM D695-23 dedicated to the determination of the compressive stress and strain), using LBG100 universal testing machine (Figure 11). The printed specimens were compressed according to Figure 12. The Figure 13 shows the macroscopic images of a printed specimen before and after the compression test, according ASTM D695 [27]. The testing machine was not restricted regarding the applied force. Most of the pieces were pressed by 80-90 kN force. The material was deformed under the action of force. At the end of the test, the specimen structure was elastic enough to show a thickness recovery, according EN 2850:2020 [28].

Figure 14 a and b show examples of curves recorded during the compression test of a traditionally printed specimen and a hybrid heated printed specimen.

The compressive force vs. transverse displacement curve resulting from the compression test of PLA printed under traditional conditions, without changing the cooling rate, has a steeper slope than the curve obtained for samples cooled more slowly, which shows a higher initial stiffness of the material (higher elastic modulus), which reflects an amorphous structure with internal stresses.

Figure 11. LBG A009 (TC100) testing machine

Figure 12. Compression testing process

Figure 13. Specimen before and after the compression test

It shows a sudden failure and relatively rapid fracture (more brittle behaviour), which indicates a lack of crystallization and a disordered molecular structure. This condition could be explained by the fact that the rapid cooling in the classic FFF printing process prevents the formation of crystals, and the material remains predominantly amorphous, with high internal stresses. This leads to brittle behaviour. In the case of the slower cooling sample curve, the elastic modulus is initially lower, suggesting a flexible material.

After a higher initial deformation, the curve shows a gradual hardening (strain hardening) and a higher resistance to deformation. One explanation is that slow cooling allows the relaxation of internal stresses and the partial crystallization of the material. Crystallization creates ordered regions in the polymer, which gives it a better resistance to large deformations and prevents sudden fracturing. The differences between the behaviours have three aspects: initial stiffness, resistance to large deformations and fracture behaviour. The amorphous structure of the rapidly cooled material is initially stiffer, while the partially crystallized (slowly cooled) material is more flexible.

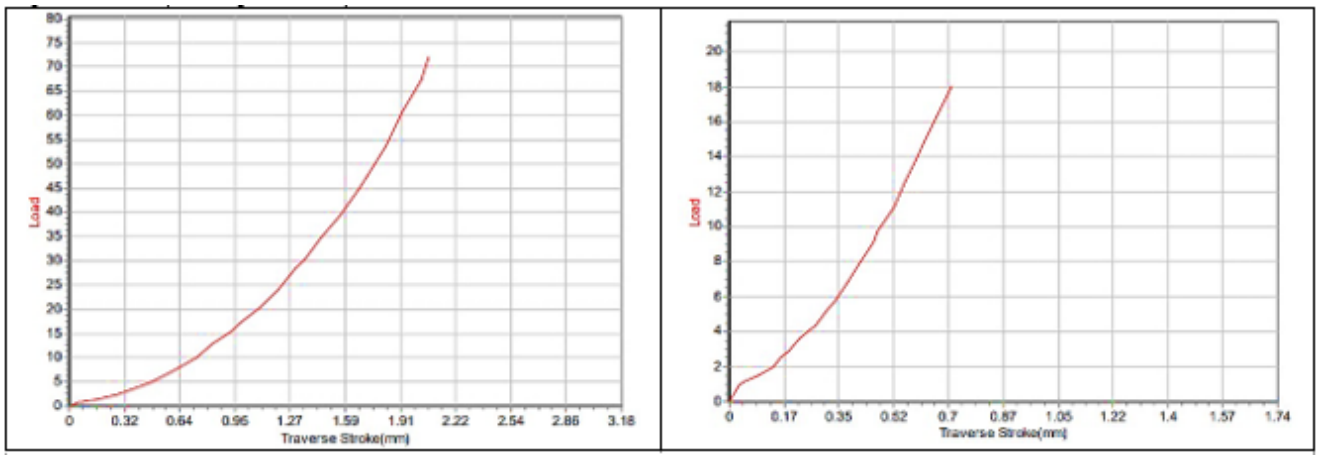

a. Compression test curve for the sample without heat addition

b. Compression test curve for the sample with heat addition (120ºC)

Figure 14. Curves of compressive force against the traverse displacement

At the same time, the slowly cooled material has a more ductile behaviour, with a greater capacity to withstand significant deformations before failure. In terms of fracture, the rapidly cooled material (classic FFF) fails abruptly, while the slowly cooled material shows a more progressive behaviour, due to the strength conferred by the partially crystalline structure. These differences highlight the importance of cooling conditions on the mechanical properties of PLA parts manufactured by 3D printing.

4. Conclusions

The present experimental findings demonstrate that the incorporation of a supplementary thermal source, in the form of a controlled hot air stream during the FFF process, has a significant impact on both thermal behaviour and mechanical performance of printed polymer parts, particularly for PLA and ABS materials. Measurements indicate that the dimensional deviations induced by the hybrid thermal setup remain below 0.25 mm in both width and height for rectangular samples of 50×20×5 mm. This confirms that the introduction of the secondary thermal field does not compromise dimensional fidelity, even when applied continuously at moderate temperatures (100–140°C). Morphological analysis performed via SEM reveals substantial improvement in interlayer fusion and surface regularity. Samples fabricated without hot air assistance display characteristic defects, such as interfacial gaps and surface roughness, attributable to insufficient thermal diffusion across layers. In contrast, samples subjected to a hot air stream at 120°C exhibit homogenous stratification, reduced interlayer discontinuities, and a markedly smoother surface profile. This enhancement is attributed to the extended residence time of the polymer in its viscoelastic state, allowing more complete molecular interdiffusion between adjacent layers.

DSC analyses reinforce the hypothesis of improved structural development. For PLA samples processed without heat assistance, the glass transition temperature (T_g) was recorded at 64.4°C, while for samples with thermal aid, T_g increased slightly to 65.9°C. The cold crystallisation peak shifted from 89.8°C to 86.9°C, and the associated enthalpy (ΔH_c) dropped from $31.7\,J/g$ to $22.5\,J/g$, indicating that partial crystallisation occurs during deposition when the polymer is kept in a semi-molten state for longer durations. Similarly, the melting temperature (T_m) remained close to 157.4°C, but the enthalpy of fusion (ΔH_m) increased, implying the formation of more stable crystalline domains.

The theoretical explanation is grounded in thermal diffusion principles and viscoelastic behaviour. According to Fourier's law of heat conduction ($q = -k\nabla T$), the introduction of an external hot air stream reduces thermal gradients within the deposited material. This effect prolongs the dwell time in the viscoelastic range (between T_g and T_m), allowing polymer chains to reconfigure and interdiffuse. As the cooling rate decreases, the critical temperature for molecular motion is surpassed more slowly, allowing enhanced relaxation and segmental mobility. These dynamics result in improved interfacial bonding and morphological continuity across deposition paths.

Thermomechanical analysis of the dynamic mechanical behaviour confirms that hybrid-heated PLA and ABS samples exhibit improved damping properties and reduced internal stress accumulation. The $Tan\,\delta$ peak, typically associated with the alpha-transition, narrows and shifts to lower temperatures, indicating increased structural order. Moreover, the storage modulus (E') for PLA increases by over 15% in the thermally assisted samples at room temperature, while the loss modulus (E'') also increases in the rubbery plateau region. This suggests that the hybrid system promotes a better balance between stiffness and energy dissipation capacity, which is crucial for load-bearing applications.

Compression tests show that thermally stabilised samples resist fracture more effectively, with up to 28% higher strain before failure and a more progressive stress–strain curve. Samples without hot air exposure exhibit a brittle response, with a linear elastic regime followed by abrupt failure, indicative of poor interlayer bonding and residual stress concentration.

In conclusion, the integration of a hot air thermal source in the FFF process plays a pivotal role in enhancing the interlayer adhesion, structural organisation, and thermomechanical stability of printed polymer components. The system enables control over the cooling rate, modulates thermal gradients, and supports the development of favourable crystalline structures. These improvements do not compromise dimensional accuracy and open new opportunities for the design of high-performance FFF systems with hybrid thermal regulation.

References

1.AL-MALIKI, J. Q., AL-MALIKI, A. J. Q., The Processes and Technologies of 3D Printing, *International Journal of Advances in Computer Science and Technology*, **4** (10), 2015, 161-165.

2.MUNSCH, M., AMPOWER REPORT 2022 - Management Summary, AMPOWER GmbH & Co. KG, Hamburg, 2021, 4-5.
3.VIDAKIS, N., KECHAGIAS, J. D., PETOUSIS, M., VAKOUFTSI, F., MOUNTAKIS, N., The effects of FFF 3D printing parameters on energy consumption, *Materials and Manufacturing Processes*, 2022.
4.KECHAGIAS, J. D., VIDAKIS, N., PETOUSIS, M., MOUNTAKIS, N., A multi-parametric process evaluation of the mechanical response of PLA in FFF 3D printing, *Materials and Manufacturing Processes*, 2022.
5.CUIFFO, M. A., SNYDER, J., ELLIOTT, A. M., ROMERO, N., KANNAN, S., HALADA, G. P., Impact of the Fused Deposition (FDM) Printing Process on Polylactic Acid (PLA) Chemistry and Structure, *Appl. Sci.* **7**, 2017, 579.
6.SAVU, S.V., SAVU, I.D., CIUPITU, I., Thermal Analysis to Evaluate Ageing Process in Heated Tool and Electrofusion Welding of Polymer Pipes, *Advanced Materials Research, Modern Technologies in Industrial Engineering*, vol. **837**, 2014, 190.
7.VALERGA, A. P., BATISTA, M., FERNANDEZ-VIDAL, S. R., GAMEZ, A. J., Impact of Chemical Post-Processing in Fused Deposition Modelling (FDM) on Polylactic Acid (PLA) Surface Quality and Structure, *Polymers*, **11**, 2019.
8.VAES, D., VAN PUYVELDE, P., Semi-crystalline feedstock for filament-based 3D printing of polymers. Progress in *Polymer Science*, **118**, 2021.
9.LIAO, Y., LIU, C., COPPOLA, B., BARRA, G., DI MAIO, L., INCARNATO, L., LAFDI, K., Effect of Porosity and Crystallinity on 3D Printed PLA Properties. *Polymers*, **11**, 2019, 1487.
10.KECHAGIAS, J., CHAIDAS, D., VIDAKIS, N., SALONITIS, K., VAXEVANIDIS, N. M., Key parameters controlling surface quality and dimensional accuracy: a critical review of FFF process, *Materials and Manufacturing Processes*, **37** (9), 2022, 963-984
11.SAVU, I.D., SAVU, S.V., SEBES, G., Preheating and heat addition by LASER beam in hybrid LASER-ultrasonic welding, *J. of Thermal analysis and calorimetry*, **111**, 2013, 1221-1226
12.DIMONIE, D., DRAGOMIR, N., TRUSCA, R., JECU, L., CONSTANTIN, M., GHIUREA, M., The 3D/4D Printing Defects and Their Influence on the Functional Behavior of the Achieved Items from Renewable Compounds. (I), *Mater. Plast.*, **58**(2), 2021, 18-32
13.SAVU, I.D., DA FONSECA PESTANA ASCENSO PIRES, I., SAVU, S. V., CIORNEI, M., SIMION, D., OLEI, A. B., Specific behaviour of Sn-Zn low fusion alloy used as material for filament dedicated to FDM printing process, *Acta Technica Napocensis, Seried-Applied Mathematics Mechanics and Engineering*, **64**, 2021, 423-428.
14.RIPANU, M. I., MIHALACHE, A. M., SLATINEANU, L., MARES, M., ANDRUSCA, L., HRITUC, A., DODUN, O., NAGIT, G., COTEATA, M., RADULESCU, B., Tensile Strength of Threaded Rods Made by 3D Printing of Polymeric Material, *Mater. Plast.*, **58**, 2021, 9-18.
15.WACH, R.A., WOLSZCZAK, P., ADAMUS-WLODARCZYK, A., Enhancement of Mechanical Properties of FDM-PLA Parts via Thermal Annealing. *Macromol. Mater. Eng.*, **303**, 2018.
16.HSUEH, M.-H., LAI, C.-J., CHUNG, C.-F., WANG, S.-H., HUANG, W.-C., PAN, C.-Y., ZENG, Y.-S., HSIEH, C.-H., Effect of Printing Parameters on the Tensile Properties of 3D-Printed Polylactic Acid (PLA) Based on Fused Deposition Modelling, *Polymers*, **13**, 2021.
17.DOBRESCU, T., PASCU, N.-E., JIGA, G., SIMION, I., ADIR, V., ENCIU, G., TUDOSE, D. I., Tensile Behavior of PLA and PLA Composite Materials Under Different Printing Parameters, *Mater. Plast.*, **56**, 2019, 18-32
18.ENACHE, I. C., CRISTINA, I. M., CHIVU, O. R., MATES, I., IONITA, E., GEAMBASU, G., The Influence of 3D Printing Parameters on the Mechanical Behavior of PLA, *Mater. Plast.*, **61**(1), 2024, 82-92
19.ANDREU, A., KIM, S., DITTUS, J., FRIEDMANN, M., FLEISCHER, J., YOON, Y. J., Hybrid material extrusion 3D printing to strengthen interlayer adhesion through hot rolling, *Additive Manufacturing*, **55**, 2022.

20.STANCIU, N.-V., ROSCULET, R., FETECAU, C., TAPU, C., Forensic Facial Reconstruction Using 3D Printing, *Mater. Plast.*, **57**(4), 2020, 248-257.
21.LEE, C.-Y., LIU, C.-Y. The Influence of Forced-Air Cooling on a 3D Printed Part Manufactured by Fused Filament Fabrication. Additive Manufacturing. **25**, 2018.
22.VELGHE, I., BUFFEL, B., VANDEGINSTE, V., THIELEMANS, W., DESPLENTERE, F., Review on the Degradation of Poly(lactic acid) during Melt Processing. *Polymers* **15**, 2023.
23.***EN ISO 1923:1999 Cellular plastics and rubbers - Determination of linear dimensions
24.***ASTM E794-06(2018) Standard Test Method for Melting and Crystallization Temperatures by Thermal Analysis
25.***ISO 6721-11:2019 Plastics - Determination of dynamic mechanical properties. Part 11: Glass transition temperature
26.***ISO 11357-1:2023 Plastics - Differential scanning calorimetry (DSC). Part 1: General principles
27.***ASTM D695-23 Standard Test Method for Compressive Properties of Rigid Plastics
28.***EN 2850:2020 Aerospace series - Carbon fibre thermosetting resin - Unidirectional laminates - Compression test parallel to fibre direction

Manuscript received: 30.02.2024